Holographic photoelectrochemical etching of diffraction gratings in *n*-InP and *n*-GaInAsP for distributed feedback lasers

R. M. Lum, A. M. Glass, F. W. Ostermayer, Jr.,[a] P. A. Kohl,[a] A. A. Ballman, and R. A. Logan
AT&T Bell Laboratories, Holmdel, New Jersey 07733

(Received 13 June 1984; accepted for publication 28 July 1984)

Direct photoelectrochemical (PEC) etching of diffraction gratings on *n*-InP and *n*-GaInAsP in a 2-*M* HF/0.5-*M* KOH solution has been demonstrated using laser interference holography. Development of a maskless technique for producing gratings has potential application in the fabrication of distributed feedback lasers which are currently made by a multistep photoresist process. Submicron diffraction gratings having a period of 0.5 μm, corresponding to second-order feedback in GaInAsP at $\lambda = 1.55\ \mu$m, have been achieved. Measurements were obtained on the exposure characteristics, diffraction efficiency, and PEC etching sensitivity of gratings produced in InP and GaInAsP as a function of the writing beam intensity, laser wavelength, material doping level, and grating spatial frequency. For grating frequencies greater than 100 mm^{-1} the sensitivity was observed to decrease approximately as the inverse square of the spatial frequency. In addition, undoped InP and GaInAsP exhibited significantly lower sensitivities than *n*-doped material.

INTRODUCTION

Direct generation of submicron patterns onto semiconductor surfaces is of great interest for the fabrication of distributed feedback (DFB) lasers. The intrinsically stable single-longitudinal mode operation of DFB lasers makes them suitable for use in high bit rate (GHz range) fiber-optic data transmission systems. Current research is centered on GaInAsP/InP DFB lasers in the 1.55-μm wavelength region[1–4] where silica fibers exhibit minimum attenuation. DFB lasers are fabricated by producing a periodic surface corrugation in close proximity to the active region. Feedback occurs by Bragg scattering from the corrugation grating and is thus distributed throughout the laser structure.[5] The lasing wavelength is determined by the period of the DFB grating. For first-order feedback at 1.55 μm in GaInAsP a grating period of aproximately 0.23 μm is required.

The grating corrugations are typically formed by holographic[6,7] or electron beam[8] exposure of a photoresist mask followed by ion beam milling[9,10] or wet chemical etching[11] of the semiconductor surface. More recently several direct writing techniques have been investigated. High intensity (>10 kW/cm^2) pulsed laser annealing has been used to write gratings in GaP,[12] GaAs,[13] and Ge[14] substrates. At intermediate intensities (10–1000 W/cm^2) gas-phase laser photolysis has been used to produce surface relief features in GaAs and InP with a spatial resolution of about 1 μm.[15] Finally, low intensity (<1 W/cm^2) laser induced liquid-phase etching has been used to write submicron patterns in GaAs by photogeneration of reactive species in the etchant solution[16] and minority carriers in the semiconductor.[17–20] In Ref. 19, work with CdS and Fe-doped semi-insulating InP was also briefly mentioned.

Measurements are reported here on the direct holographic etching of diffraction gratings in InP and GaInAsP using a photoelectrochemical (PEC) technique.[21,22] In this technique the semiconductor sample is placed in an electrolyte and biased to form a depletion region at the surface. Etching is controlled by the light intensity at the surface and for *n*-type materials occurs by an oxidative decomposition reaction involving photogenerated holes.

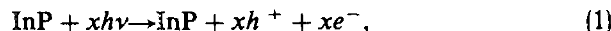

$$\mathrm{InP} + xh\nu \rightarrow \mathrm{InP} + xh^{+} + xe^{-}, \qquad (1)$$

$$\mathrm{InP} + xh^{+} \rightarrow \mathrm{In(III)} + \mathrm{P(III)} + (6-x)e^{-}. \qquad (2)$$

In the above reaction x is the number of photons participating in the oxidation of one InP molecule and $6-x$ is the number of nonphotogenerated electrons.

Direct holographic exposure of the sample produces a light interference pattern with a sinusoidal spatial intensity variation across the sample surface. Selective photoetching results since the light to dark etch rate ratio is greater than 100:1. In this paper we present data on the exposure characteristics, efficiency, and spatial frequency response of holographic surface relief gratings produced in undoped InP ($n = 3\times10^{15}$ cm^{-3}), S-doped *n*-InP ($n = 6\times10^{18}$ cm^{-3}), undoped GaInAsP ($n\sim5\times10^{16}$ cm^{-3}), and Sn-doped *n*-GaInAsP ($n\sim1\times10^{18}$ cm^{-3})

EXPERIMENT

Photoelectrochemical etching of InP and GaInAsP was performed in a 2-*M* HF/0.5-*M* KOH solution which had previously been found[22] to give the smoothest etched surfaces on (100) InP. The sample potential was controlled between 0.2–0.5 V versus a saturated calomel electrode. A schematic of the laser interferometer arrangement used to produce the gratings is shown in Fig. 1. Light from a laser source is split into two nearly equal intensity beams which then intersect at the sample surface with an angle 2θ. The beams were polarized perpendicular to the plane of incidence. The interference fringe pattern produced by the intersecting beams results in a sinusoidal variation in the irradiance at the sample surface of

[a] AT&T Bell Laboratories, Murray Hill, New Jersey 07974.

 0021-8979/85/010039-06$02.40 © 1984 American Institute of Physics

Downloaded 26 Jan 2008 to 130.207.50.192. Redistribution subject to AIP license or copyright; see http://jap.aip.org/jap/copyright.jsp

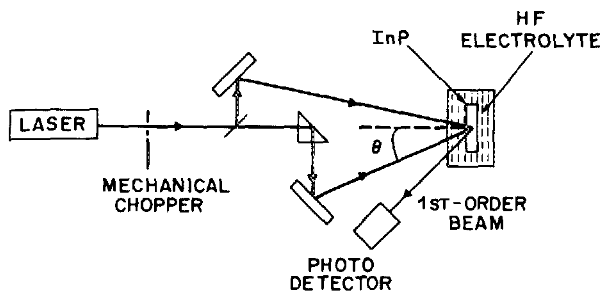

FIG. 1. Schematic of laser interferometer apparatus.

$$I(x) = 2I_i\left(1 + \cos\frac{2\pi x}{a}\right). \qquad (3)$$

I_i is the incident intensity in each beam and a is the fringe spacing which is given by the Bragg relationship

$$a = \frac{\lambda_0}{2n_e \sin\theta}, \qquad (4)$$

where λ_0 is the free-space wavelength and n_e is the index of refraction of the electrolyte.

The maximum rate of material removal from the exposed sample occurs at the maxima of the interference pattern due to oxidation induced by photogenerated holes. The resulting variation in surface relief $2\Delta d$ produces a corresponding phase modulation in the light reflected from the sample of

$$\phi_1 = \frac{4\pi\Delta d}{\lambda \cos\theta}. \qquad (5)$$

Since Δd is proportional to the intensity given in Eq. (3), the phase shift also exhibits a sinusoidal modulation given by

$$\phi(x) = \phi_0 + \phi_1 \cos\frac{2\pi x}{a}. \qquad (6)$$

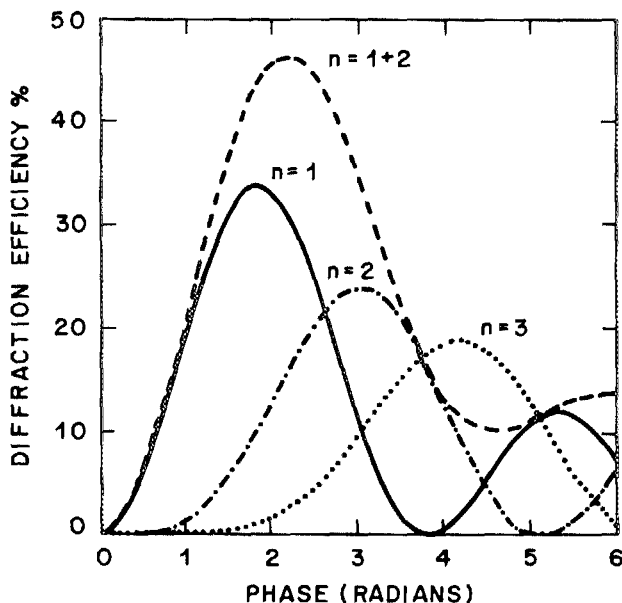

FIG. 2. Calculated diffraction efficiency for $n = 1$–3 for a thin phase hologram.

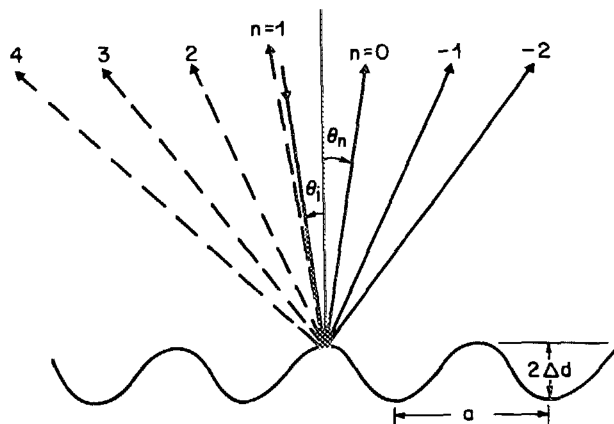

FIG. 3. Schematic of diffracted beams from a sinusoidal surface.

Surface relief gratings produced in this manner are classified as thin phase holograms, and have been extensively studied.[23–28]

Light incident on a sinusoidal phase-grating will be scattered into the various diffraction orders $\pm n$ with an efficiency[23]

$$\eta = \frac{I_n}{I_i} = J_n^2(\phi_1), \qquad (7)$$

where I_n is the intensity of the nth diffracted order and $J_n(\phi_1)$ is the nth order Bessel function. The calculated efficiencies for the first few diffracted orders are plotted in Fig. 2 as a function of the phase difference ϕ_1 and the surface relief $2\Delta d$ for $\lambda_0 = 0.6328\ \mu$m.

In these experiments the $n = -1$ diffracted beam was selected to monitor the growth of the grating with time. Unlike the $n = +1$ image, it is spatially separated from the zero-order or reflected image of the second incident beam as shown schematically in Fig. 3. This eliminated the necessity of a second readout laser beam at different wavelength. The incident laser beam was chopped at 150 Hz and the intensity of the diffracted beam was measured with a photodetector using phase-sensitive detection. An interferometric technique was used to monitor continuously the stability of the holographic recording system during an exposure. The grating period was changed by varying the angle between the two incident beams. The wavelength and power density of the

TABLE I. Range of values used for the wavelength and power density of the incident beam during holographic exposures. Also indicated is the absorption length of the incident radiation in InP.

Laser source	Wavelength (μm)	Irradiance (mW/cm^2)	Absorption length in InP (μm)
HeNe	0.6328	1–30	0.2
Ar^+	0.488	5–25	0.08
HeCd	0.4416	50–350	0.05

Downloaded 26 Jan 2008 to 130.207.50.192. Redistribution subject to AIP license or copyright; see http://jap.aip.org/jap/copyright.jsp

incident beam were varied over the range 0.442–0.633 μm and 1–350 mW/cm^2, respectively, as indicated in Table I. With this experimental setup direct measurements of the grating formation rate could be obtained.

RESULTS AND DISCUSSION

Although the $n = -1$ diffracted image of one incident beam coincides with the $n = +2$ image of the second incident beam, contributions from the second-order image are negligible during the initial growth stage of the grating. This is illustrated in Fig. 4 by the diffraction efficiency data obtained for 8.5 and 1.5 μm period gratings in n-InP. The data were corrected for the reflection losses from the sample, sample cell and electrolyte. The dashed curves are the calculated fraction of the total radiant intensity which appears in the first-order diffracted beam, and in the sum of the first- and second-order diffracted beams. It is evident from Fig. 4 that the observed signals reach a saturation level before contributions from the second-order beam become significant.

Diffracted beams out to seventh-order were observed for the 8.5 μm grating and are shown in Fig. 5 together with the calculated diffraction intensities. Comparison of the observed and calculated diffraction efficiencies of Figs. 4 and 5 indicate that, at low exposure, the gratings produced by this method are indeed sinusoidal. A scanning electron photomicrograph of the cross-sectional profile of a 1.5 μm grating having a depth of 3500 Å is shown in Fig. 6.

The material exposure characteristics can be determined from the diffracted beam intensity data. For ideal materials the first-order diffraction efficiency η is a quadratic function of the exposure E_0,[24] so that

$$\eta^{1/2} = SE_0V, \quad (8)$$

where E_0 is the average exposure $(2I_i t)$, V is the fringe visibility or irradiance modulation ($V = 1$ for equal intensity incident beams) and S is the holographic sensitivity. The sensitivity is a measure of the rate at which the grating amplitude increases during a given exposure. The data of Fig. 4 are

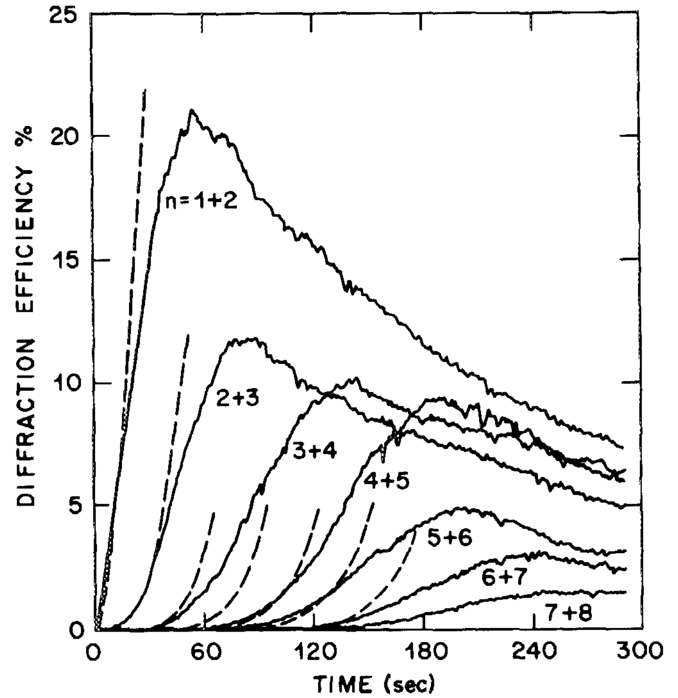

FIG. 5. Measured intensities of diffracted beams out to seventh-order from 8.5 μm gratings in n-InP.

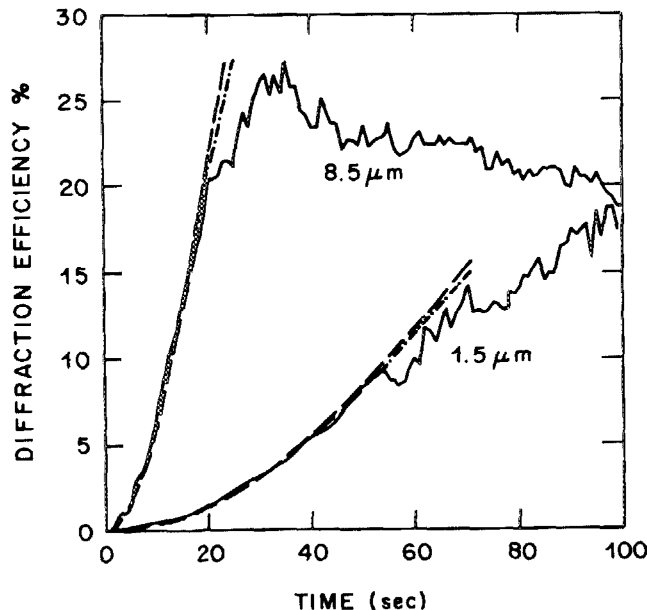

FIG. 4. Measured intensities of the first-order diffracted beams from 1.5 and 8.5 μm gratings in n-InP. Calculated curves for the first-order diffracted beam (– · –) and the sum of the first- and second-order beams (– –) are also shown.

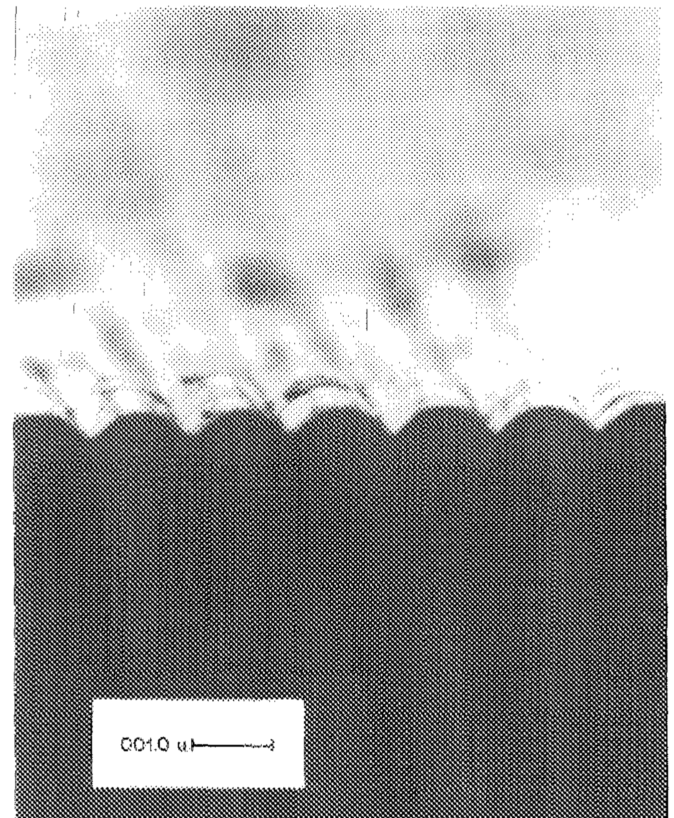

FIG. 6. Scanning electron photomicrograph of the cross-sectional profile of a 1.5 μm grating in n-InP having a depth of 3500 Å.

Downloaded 26 Jan 2008 to 130.207.50.192. Redistribution subject to AIP license or copyright; see http://jap.aip.org/jap/copyright.jsp

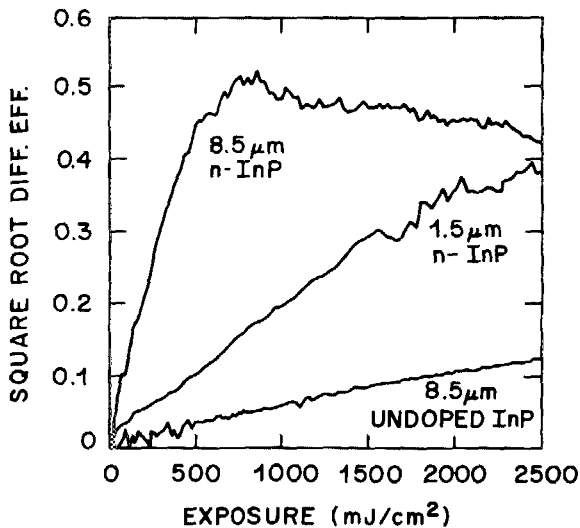

FIG. 7. Plots of $\eta^{1/2}$ vs exposure for 1.5 and 8.5 μm gratings in n-InP and an 8.5 μm grating in undoped InP.

replotted in Fig. 7 in terms of $\eta^{1/2}$ vs exposure. Also shown are the corresponding exposure data obtained for an 8.5 μm grating in undoped InP. The exposure characteristics are seen to vary with both the spatial frequency of the grating and the doping level of the n-InP substrate. The grating efficiency can be related to grating depth through Eqs. (5) and (7). This enables real-time monitoring of the grating depth to be performed during an exposure. Calculated values for the grating depth agree well with interference microscopy measurements obtained on gratings where the exposure was stopped once the peak diffraction efficiency was obtained.

The holographic sensitivity S was determined from the slope of the linear portion of the exposure curves using digital data smoothing and least-squares analysis as shown in Fig. 8. Sensitivity measurements were obtained for diffrac-

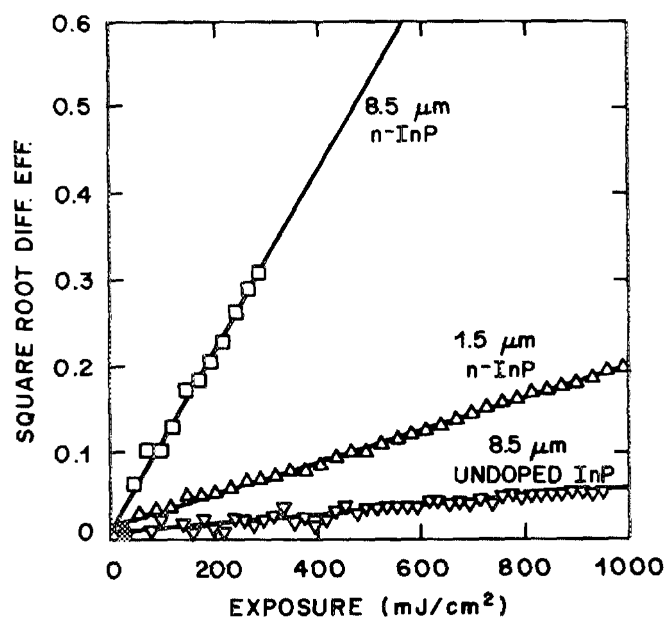

FIG. 8. Measurements of the holographic sensitivity from the linear portion of the $\eta^{1/2}$ vs exposure curves for gratings in n-InP and undoped InP.

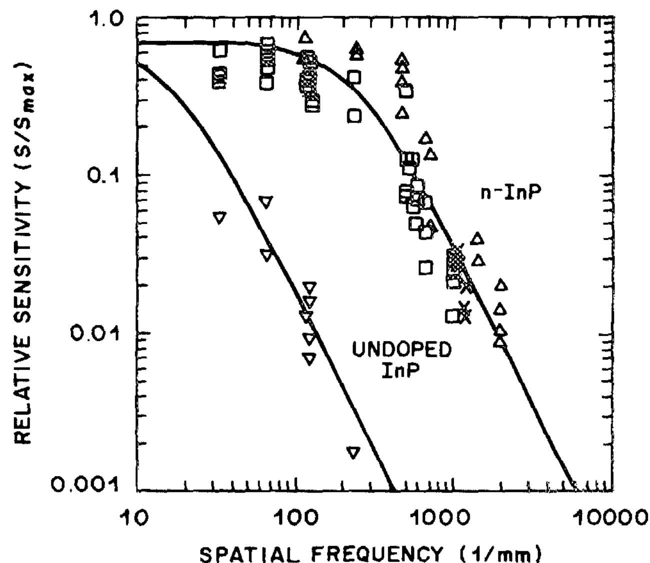

FIG. 9. Spatial frequency response of gratings in n-InP and undoped InP for incident beam wavelengths of 0.4416 μm (△), 0.488 μm (×), and 0.6328 μm (□, ▽).

tion gratings produced in undoped and n-type InP over the spatial frequency range 30–2000 mm^{-1}. The spatial frequency response of the two materials is plotted in Fig. 9. At low spatial frequency the measured sensitivity of n-InP is close to the value calculated (2.7×10^{-3} cm^2/mJ) based on the PEC etching rate determined from the measured photocurrent. However, at spatial frequencies greater than 100 mm^{-1} the sensitivity decreases approximately as the inverse square of the spatial frequency. In addition, undoped InP exhibits significantly lower sensitivities. Similar behavior was observed for GaInAsP as shown in Fig. 10. The spatial frequency response data suggest that the photoetching sensitivity of these materials is limited by lateral diffusion of the photogenerated holes. Finally, over the wavelength range

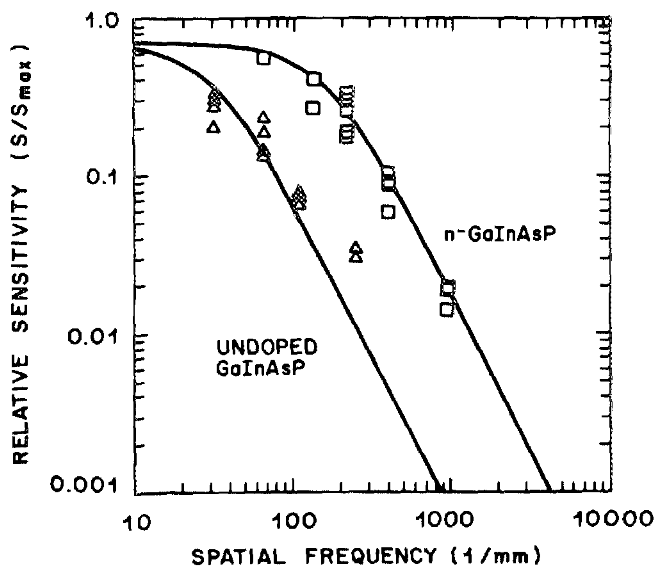

FIG. 10. Spatial frequency response of gratings in n-GaInAsP and undoped GaInAsP for an incident beam wavelength of 0.6328 μm.

Downloaded 26 Jan 2008 to 130.207.50.192. Redistribution subject to AIP license or copyright; see http://jap.aip.org/jap/copyright.jsp

studied the absorption length of the incident radiation in InP varies by a factor of four (cf. Table I). However, no wavelength dependence was observed in the sensitivity data of Fig. 9.

The differential material removal rate is determined by the variation of the hole density at the crystal-electrolyte interface. The surface relief of the grating relative to the average depth etched is therefore detemined by the ratio of the amplitude of the spatial modulation of the hole concentration Δp to its average value $\bar{p}$. Due to absorption of the incident light within the semiconductor the photogeneration rate of holes decays exponentially perpendicular to the surface, as well as varying sinusoidally in the direction parallel to the interface. The photogenerated holes both drift, under the influence of the space-charge field, and diffuse to the interface where reaction with the electrolyte results in dissolution of the surface according to Eq. (2).

We have incorporated these effects into a two-dimensional hole transport model.[29] Good agreement between the quantitative predictions of this model and the experimental data is obtained by using the reaction velocity of the decomposition reaction [Eq. (2)] as a fitting parameter. In Figs. 9 and 10 theoretical curves have been fitted to the data using the values listed in Table II for the reaction velocity. Despite the large differences in carrier concentration and experimental behavior, the values of the reaction velocity are close to each other as would be expected. For these values of the reaction velocity the theoretical curves are insensitive to the value of the hole diffusion length within the range of published measurements.[30–35] This results from the fact that the quantum efficiency for the decomposition reaction is 100% to within experimental error, indicating that the holes react at the surface before recombining. Of course the value of the diffusion coefficient does affect the result. The reaction velocities in Table II are based on the tabulated value of 3.9 cm^2/sec for InP.[36]

For the values of the reaction velocity listed in Table II the grating resolution is limited by diffusion that occurs in a narrow region of high hole concentration that forms within the space-charge layer at the surface, rather than by diffusion from their point of generation. This explains the relatively weak dependence observed in the grating sensitivity data on the wavelength of the incident radiation. Increasing the reaction rate constant would decrease the hole concentration and the diffusion in the surface region. The quantitative predictions from the model indicate that a substantial improvement in resolution is, in principle, obtainable. A more detailed discussion of the implications of this model for PEC etching of submicron gratings is contained in Ref. 29.

TABLE II. Experimental values of the reaction velocity for surface dissolution in the 2-*M* HF/0.5-*M* KOH solution during exposure of *n*-InP and *n*-GaInAsP.

Material	Doping level (cm^{-3})	Reaction velocity (cm/sec)$\times 10$
n-InP	3×10^{15}	1.4
	6×10^{18}	3.5
n-GaInAsP	5×10^{16}	0.93
	1×10^{18}	5.5

CONCLUSION

Direct photoelectrochemical etching of submicron patterns using a laser interference technique has been investigated for InP and GaInAsP materials. Diffraction gratings with periods as short as 0.5 μm were produced. Measurements of the exposure characteristics indicate that the modulation amplitudes of the gratings decrease with increasing spatial frequency. At high spatial frequency selective photoetching appears to be limited by surface hole diffusion.

For placement of DFB corrugations in the InP substrate, the decreased modulation amplitude is not a severe restriction and application of the PEC technique for direct generation of gratings in the fabrication of DFB lasers is possible. Formation of the grating structure in quaternary epilayers (0.1–0.2 μm thickness), however, is limited to low spatial frequencies because of the rapid decrease in modulation amplitude with grating frequency. Direct PEC etching of submicron gratings has promise for eliminating the complexities and material damage associated with conventional lithographic techniques. Finally, laser-induced PEC etching has potential as a sensitive surface probe since at low incident beam intensities etching of the first few angstroms occurs over a time interval of 1–5 sec. Sampling the surface on this scale should enable characterization of various surface effects.

[1] T. Matsuoka, H. Nagai, Y. Itaya, Y. Naguchi, Y. Suzuki, and T. Ikegami, Electron. Lett. **18**, 27 (1982).
[2] S. Akiba, K. Utaka, K. Sakai, and Y. Matsushima, Electron. Lett. **18**, 77 (1982).
[3] A. W. Nelson, L. D. Westbrook, and J. S. Evans, Electron. Lett. **19**, 34 (1983).
[4] K. Utaka, K. Kobayashi, and Y. Suematsu, IEEE J. Quantum Electron. Lett. **QE-17**, 651 (1981).
[5] H. Kogelnik and C. V. Shank, Appl. Phys. Lett. **18**, 152 (1971).
[6] M. J. Beesley and J. G. Castledine, Appl. Opt. **9**, 2720 (1970).
[7] L. F. Johnson, G. W. Kammlott, and K. A. Ingersoll, Appl. Opt. **17**, 1165 (1978).
[8] L. D. Westbrook, A. W. Nelson, and C. Dix, Electron. Lett. **18**, 863 (1982).
[9] H. L. Brown, E. Garmire, S. Somekh, H. Stoll, and A. Yariv, Appl. Opt. **12**, 455 (1973).
[10] C. V. Shank and R. V. Schmidt, Appl. Phys. Lett. **23**, 154 (1973).
[11] T. Saitoh, O. Mikami, and H. Nakogome, Electron. Lett. **18**, 408 (1982).
[12] K. P. Alum, Y. V. Kovalchuk, G. V. Ostrovskaya, E. L. Portnoi, V. I. Smilgyairchyus, and I. A. Sokolov, Sov. Tech. Phys. Lett. **7**, 633 (1981).
[13] P. Fauchet and A. E. Siegman, Appl. Phys. Lett. **40**, 824 (1982).
[14] D. J. Ehrlich, S. R. J. Brueck, and J. Y. Tsao, Appl. Phys. Lett. **41**, 630 (1982).
[15] D. J. Ehrlich, R. M. Osgood, and T. F. Deutsch, Appl. Phys. Lett. **36**, 698 (1980).
[16] R. W. Haynes, G. M. Metze, V. G. Kreismanis, and L. F. Eastman, Appl. Phys. Lett. **37**, 344 (1980).
[17] L. V. Belyakov, D. N. Goryachev, M. N. Mizerov, and E. L. Portnoi, Sov. Tech. Phys. **19**, 837 (1974).
[18] Zh. I. Alferov, D. N. Goryachev, S. A. Gurevich, M. N. Mizerov, E. L. Portnoi, and B. S. Ryvkin, Sov. Phys. Tech. Phys. **21**, 857 (1976).
[19] R. M. Osgood, Jr., A. Sanchez-Rubino, D. J. Ehrlich, and V. Danen, Appl. Phys. Lett. **40**, 391 (1982).
[20] D. V. Podlesnik, H. H. Gilgen, and R. M. Osgood, Jr., Appl. Phys. Lett. **43**, 1083 (1983).
[21] F. W. Ostermayer, Jr. and P. A. Kohl, Appl. Phys. Lett. **39**, 76 (1981).
[22] P. A. Kohl, C. Wolowodiuk, and F. W. Ostermayer, Jr., J. Electrochem. Soc. **130**, 2288 (1983).

Downloaded 26 Jan 2008 to 130.207.50.192. Redistribution subject to AIP license or copyright; see http://jap.aip.org/jap/copyright.jsp

[23]H. Kogelnik, in *Symposium on Modern Optics*, edited by J. Fox (Polytechnic, New York, 1967), p. 605.
[24]L. H. Lin, J. Opt. Soc. Am. **61**, 203 (1971).
[25]J. C. Urbach and R. W. Meier, Appl. Opt. **8**, 2269 (1969).
[26]D. Meyerhofer, Appl. Opt. **10**, 416 (1971).
[27]W. J. Tomlinson, Appl. Opt. **11**, 823 (1971).
[28]L. P. Boivin, Appl. Opt. **11**, 1782 (1971).
[29]F. W. Ostermayer, Jr., P. A. Kohl, and R. M. Lum (unpublished).
[30]S. Fujita, M. Kuzuhara, M. Yagyer, and A. Sasaki, Solid State Electron. **25**, 359 (1982).
[31]L. Gouskov, C. Llinares, A. Brenac, and M. Savelli, Sol. Energy Mater. **5**, 81 (1981).
[32]S. Li, Appl. Phys. Lett. **29**, 126 (1976).
[33]V. Diadiuk, S. H. Groves, C. A. Armiento, and C. E. Hurwitz, Appl. Phys. Lett. **42**, 892 (1983).
[34]S. Sakai, M. Umeno, and Y. Amemiya, Jpn. J. Appl. Phys. **19**, 109 (1980).
[35]M. M. Tashima, L. W. Cook, and G. E. Stillman, J. Electron. Mater. **11**, 831 (1982).
[36]S. M. Sze, *Physics of Semiconductor Devices* (Wiley-Interscience, New York, 1969), p. 22.

Downloaded 26 Jan 2008 to 130.207.50.192. Redistribution subject to AIP license or copyright; see http://jap.aip.org/jap/copyright.jsp